J|A|C|S
ARTICLES

Published on Web 05/12/2009

Gyromagnetic Imaging: Dynamic Optical Contrast Using Gold Nanostars with Magnetic Cores

Qingshan Wei,[†] Hyon-Min Song,[†] Alexei P. Leonov,[†] Jacob A. Hale,[‡] Dongmyung Oh,[‡] Quy K. Ong,[†] Kenneth Ritchie,[‡] and Alexander Wei*[,†]

Department of Chemistry, Purdue University, 560 Oval Drive, West Lafayette, Indiana 47907-2084, and Department of Physics, Purdue University, 525 Northwestern Avenue, West Lafayette, Indiana 47907-2036

Received February 28, 2009; E-mail: alexwei@purdue.edu

Ⓦ **This paper contains enhanced objects available on the Internet at http://pubs.acs.org/jacs.**

Abstract: Plasmon-resonant nanoparticles with optical scattering in the near-infrared (NIR) are valuable contrast agents for biophotonic imaging and may be detected at the single-particle limit against a dark background, but their contrast is often limited in environments with high noise. Here we consider gyromagnetic imaging as a dynamic mode of optical contrast, using gold nanostars with superparamagnetic cores. The nanostars exhibit polarization-sensitive NIR scattering and can produce a frequency-modulated signal in response to a rotating magnetic field gradient. This periodic "twinkling" can be converted into Fourier-domain images with a dramatic reduction in background. We demonstrate gyromagnetic imaging of nanostars inside of tumor cells, using broadband excitation: while their time-domain signals are obscured by incoherent scattering, their Fourier-domain signals can be clearly resolved in less than a second. The gyromagnetically active nanostars do not cause a loss in viability, and can even have a mild stimulatory effect on cell growth.

Introduction

Colloidal gold nanoparticles are ideal contrast agents for biomedical optical imaging: they are chemically inert and have a long history of clinical use, and can be engineered into anisotropic forms with localized plasmon resonances in the NIR. This region is particularly favorable for the imaging of biological tissues, as shorter wavelengths (<750 nm) are extinguished by hemoglobin or other endogenous pigments, and longer wavelengths (>1300 nm) are strongly attenuated by water.[1] Several types of NIR-active Au nanoparticles are being investigated as contrast agents for various biomedical optical imaging modalities, including nanoshells,[2,3] nanorods,[4−6] and nanocages.[7] The strong absorption cross sections of these anisotropic nanoparticles can be further employed to introduce localized photothermal effects, uniting optical imaging with potential therapeutic action.[8−10] This theranostic aspect has emerged as an important paradigm within the nascent but rapidly growing field of nanomedicine.[11,12]

Plasmon-resonant nanoparticles have been widely used for resonant light scattering, which can be greater by orders of magnitude relative to objects of similar size.[13] These can also be employed as contrast agents for imaging modalities based on differential scattering such as optical coherence tomography (OCT),[3,5,7] but are challenged by structurally complex specimens with heterogeneous scattering profiles. A similar problem exists for darkfield reflectance microscopies; while single-particle scattering can be easily identified against a clean background, the detection of such particles embedded within a complex scattering environment is more challenging and requires additional mechanisms for signal enhancement, such as confocal imaging.[14]

Here we present a dynamic mode of optical contrast based on gyromagnetic imaging, in which Au nanostars with super-

[†] Department of Chemistry.
[‡] Department of Physics.

(1) Weissleder, R. *Nat. Biotechnol.* **2001**, *19*, 316–17.
(2) Wang, Y.; Xie, X.; Wang, X.; Ku, G.; Gill, K. L.; O'Neal, D. P.; Stoica, G.; Wang, L. V. *Nano Lett.* **2004**, *4*, 1689–92.
(3) Gobin, A. M.; Lee, M. H.; Halas, N. J.; James, W. D.; Drezek, R. A.; West, J. L. *Nano Lett.* **2007**, *7*, 1929–34.
(4) Wang, H.; Huff, T. B.; Zweifel, D. A.; He, W.; Low, P. S.; Wei, A.; Cheng, J.-X. *Proc. Natl. Acad. Sci. U.S.A.* **2005**, *102*, 15752–56.
(5) Oldenburg, A. L.; Hansen, M. N.; Zweifel, D. A.; Wei, A.; Boppart, S. A. *Opt. Express* **2006**, *14*, 6724–38.
(6) Eghtedari, M.; Oraevsky, A.; Copland, J. A.; Kotov, N.; Conjusteau, A.; Motamedi, M. *Nano Lett.* **2007**, *7*, 1914–18.
(7) Cang, H.; Sun, T.; Li, Z.-Y.; Chen, J.; Wiley, B. J.; Xia, Y.; Li, X. *Opt. Lett.* **2005**, *30*, 3048–50.
(8) Hirsch, L. R.; Stafford, R. J.; Bankson, J. A.; Sershen, S. R.; Rivera, B.; Price, R. E.; Hazle, J. D.; Halas, N. J.; West, J. L. *Proc. Natl. Acad. Sci. U.S.A.* **2003**, *100*, 13549–54.
(9) Tong, L.; Zhao, Y.; Huff, T. B.; Hansen, M. N.; Wei, A.; Cheng, J.-X. *Adv. Mater.* **2007**, *19*, 3136–41.
(10) Chen, J.; Wang, D.; Xi, J.; Au, L.; Siekkinen, A.; Warsen, A.; Li, Z.-Y.; Zhang, H.; Xia, Y.; Li, X. *Nano Lett.* **2007**, *7*, 1318–22.
(11) Huff, T. B.; Tong, L.; Zhao, Y.; Hansen, M. N.; Cheng, J.-X.; Wei, A. *Nanomedicine* **2007**, *2*, 125–32.
(12) Cuenca, A. G.; Jiang, H.; Hochwald, S. N.; Delano, M.; Cance, W. G.; Grobmyer, S. R. *Cancer* **2006**, *107*, 459–66.
(13) Yguerabide, J.; Yguerabide, E. E. *Anal. Biochem.* **1998**, *262*, 137–56.
(14) Javier, D. J.; Nitin, N.; Roblyer, D. M.; Richards-Kortum, R. *J. Nanophotonics* **2008**, *2*, 023506.

10.1021/ja901562j CCC: $40.75

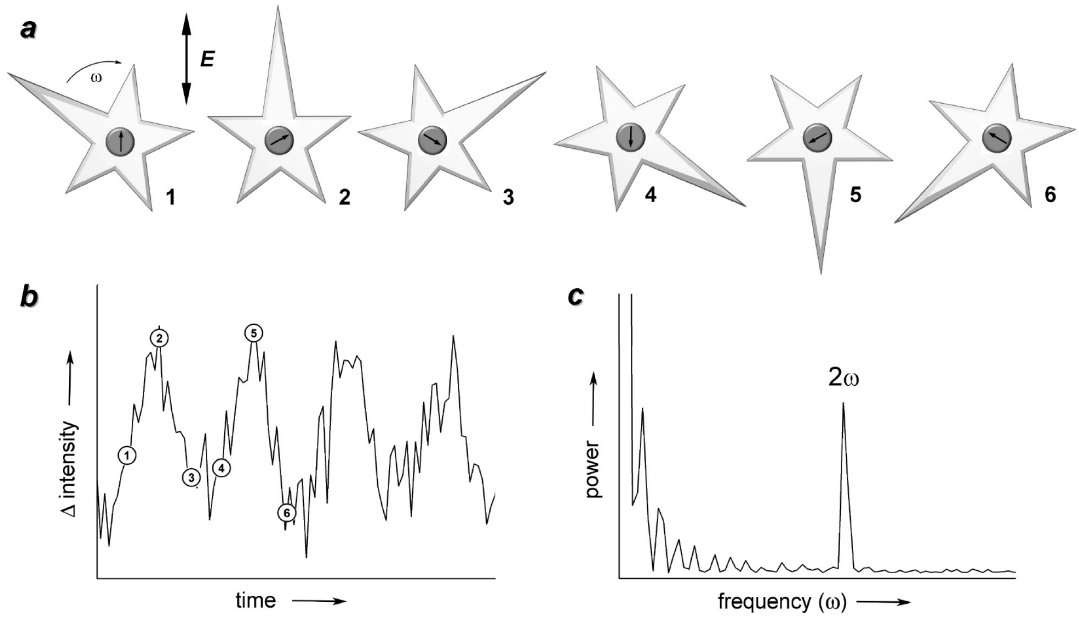

Figure 1. Dynamic optical contrast based on gyromagnetic scattering. (a) Schematic of Au nanostar with NIR-active arm and superparamagnetic core in various positions, while gyrating in response to a rotating magnetic field gradient with frequency ω; (b) time-intensity plot of polarized scattering from magnetic nanostar rotating at frequency ω (2 cycles), with reference to positions 1−6; (c) power spectrum of gyromagnetic scattering (15 cycles).

paramagnetic cores are driven by a rotating magnetic field gradient to produce periodic variations in NIR scattering intensities. Magnetically responsive agents have been shown to modulate optical signals in a temporal fashion upon exposure to a moving field gradient.[15−17] Magnetomotive scattering contrast has been applied toward *in vitro* and *in vivo* OCT imaging, based on the axial displacement of colloidal magnetite particles using a linear field gradient and subsequent modulation in signal amplitude.[17,18] Gyromagnetic imaging derives its contrast from rotational instead of translational motion, such that the signal modulation correlates directly with the frequency of magnetic field rotation to produce a characteristic periodic response (Figure 1). The frequency-modulated data can then be converted into Fourier-domain images with substantial noise reduction.[19] This brings a unique advantage to optical imaging: scatterers with signals below acceptable detection limits for conventional time-domain imaging can be rapidly elucidated when subjected to gyromagnetic imaging conditions.

Experimental Section

Synthesis of Gold Nanostars with Magnetite Cores. Fe_3O_4 nanoparticles (12.8 ± 0.9 nm) were prepared using the procedure described by Sun and co-workers.[20] Core−shell Au@Fe_3O_4 nanoparticles (15.4 ± 1.3 nm) were prepared according to the procedure described by Wang et al.,[21] then applied toward the seeded growth of gold nanostars using conditions similar to that described by Nehl et al.[22] In a typical synthesis, a freshly prepared dispersion of core−shell Au@Fe_3O_4 nanoparticles in octyl ether (1.5 mL) was diluted with hexane (2 mL), precipitated by addition of EtOH (5 mL), and then filtered and dried in air. The particles (2 mg) were redispersed in 0.5 mL of an aqueous 2.5 mM sodium citrate solution and sonicated for 20 min to produce a dark brown suspension. A portion of this seed solution (0.25 mL) was injected into a freshly prepared growth solution prepared from 0.2 M cetyltrimethylammonium bromide (CTAB, 5 mL), 4 mM $AgNO_3$ (0.9 mL), 7.8 mM $HAuCl_4$ (5 mL), and 0.078 mM ascorbic acid (0.3 mL). The reaction mixture was agitated with a vortex mixer and allowed to stand for 15 min, resulting in the formation of an iridescent blue solution. The magnetically responsive nanostars exhibited broad extinction bands centered between 800 and 900 nm, in accord with the distribution of radial plasmon resonances identified within the population of nanostars.[22]

Nanostars were cleansed of excess surfactant by treatment and partial exchange with 70-kDa sodium polystyrenesulfonate, which has recently been shown to be an effective detergent for removing CTAB from Au nanorods.[23] The nanostar dispersions were washed several times with chloroform, and could be functionalized with oligoethyleneglycol-conjugated folic acid derivatives by *in situ* dithiocarbamate formation, followed by membrane dialysis (MWCO 6000−8000) for 2 h according to a previously described procedure.[9,11] Inductively coupled plasma mass spectrometry (ICP-MS) of folate-functionalized nanostars indicates an Au and Fe content of 547 and 14.9 μg/mL, respectively, for a solution with an optical density (O.D.) of 1.0 (λ_{max} > 800 nm).

Gyromagnetic Imaging and Microscopy. The gyromagnetic behavior of the nanostars was characterized by darkfield microscopy using a linearly polarized broadband excitation source with a long-pass filter (λ_{ex} > 650 nm) or a linearly polarized NIR laser (λ_{ex} = 780 nm). An inverted optical microscope (IX-71, Olympus) optimized for darkfield imaging under epi-illumination or total internal reflectance conditions was equipped with a high-numerical aperture objective (PlanApo 100×, NA 1.4) and a dual-intensified, Peltier-cooled CCD camera (XR/Turbo-120Z ICCD, Stanford Photonics) capable of collecting pixelated images (640 × 480) at

(15) Anker, J. N.; Kopelman, R. *Appl. Phys. Lett.* **2003**, *82*, 1102–04.
(16) Aaron, J.; Oh, J.; Larson, T. A.; Kumar, S.; Milner, T. E.; Sokolov, K. V. *Opt. Express* **2006**, *14*, 12930–43.
(17) Oldenburg, A. L.; Toublan, F. J.-J.; Suslick, K. S.; Wei, A.; Boppart, S. A. *Opt. Express* **2005**, *13*, 6597–614.
(18) Oldenburg, A. L.; Gunther, J. R.; Boppart, S. A. *Opt. Lett.* **2005**, *30*, 747–49.
(19) Choma, M. A.; Sarunic, M. V.; Yang, C. H.; Izatt, J. A. *Opt. Express* **2003**, *11*, 2183–89.
(20) Sun, S. H.; Zeng, H.; Robinson, D. B.; Raoux, S.; Rice, P. M.; Wang, S. X.; Li, G. *J. Am. Chem. Soc.* **2004**, *126*, 273–79.
(21) Wang, L. Y.; Luo, J.; Fan, Q.; Suzuki, M.; Suzuki, I. S.; Engelhard, M. H.; Lin, Y.; Kim, N.; Wang, J. Q.; Zhong, C. J. *J. Phys. Chem. B* **2005**, *109*, 21593–601.
(22) Nehl, C. L.; Liao, H.; Hafner, J. H. *Nano Lett.* **2006**, *6*, 683–88.
(23) Leonov, A. P.; Zheng, J.; Clogston, J. D.; Stern, S. T.; Patri, A. K.; Wei, A. *ACS Nano* **2008**, *2*, 2481–88.

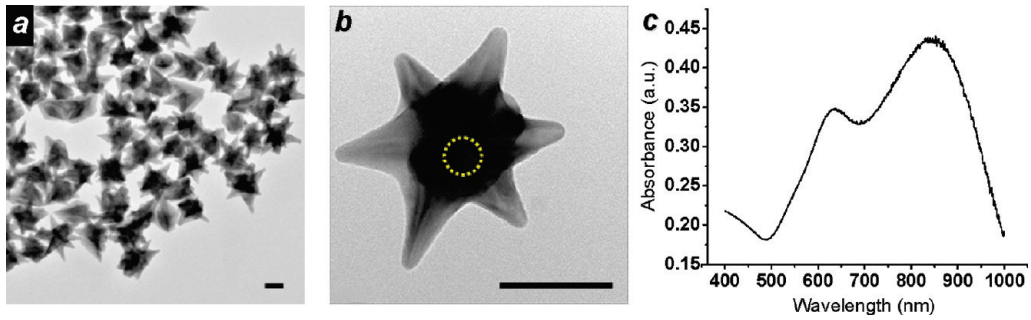

Figure 2. (a,b) TEM images of Au nanostars with superparamagnetic cores (bar = 50 nm), with approximate position of Fe_3O_4 core outlined by dashed circle; (c) optical extinction spectrum.

a rate of 120 fps. A stack of circular NdFeB magnets (0.9 cm diameter, 2 cm total height) was positioned 2 cm from the axis of an electric stirring motor, which was mechanically decoupled from the microscope stage and suspended over the imaging plane with a clearance of 0.5 cm (Scheme S1, Supporting Information). Magnetic field strengths were measured using a benchtop magnetometer (455 DSP, Lakeshore Cryotronics) equipped with a transverse Hall probe, which was placed in the imaging plane while exposed to rotating magnetic field gradients. An axial field strength (B_z) of 80 G was measured at the focal point, regardless of rotor speed.

Fourier-Domain Image Analysis. Power spectra were generated using Origin 8.0. Fourier-domain images were generated in 16-bit format using an open-source image processing and analysis program (ImageJ 1.41m) with a Fourier transform plugin. The source code was modified to include background subtraction prior to the transform, using the mean intensity of 9 pixels (3 × 3) in the upper left corner of each image. Peak signal-to-noise ratio (SNR) is defined in decibels as

$$\mathrm{SNR(dB)} = 20 \cdot \log\left(\frac{A_{ns} - A_{bk}}{\sigma_{bk}}\right)$$

where A_{ns} and A_{bk} are the mean pixel values representing peak signal and background (2 and 1054 pixels, respectively) and σ_{bk} is the standard deviation of A_{bk}.

Cell Culture and Viability Assay. KB cells (derived from a nasopharyngeal carcinoma) were cultured in folate-deficient media to induce overexpression of the cognate receptor. For TEM analysis, cells were fixed under microwave conditions using 2% glutaraldehyde in 0.1 M cacodylate buffer (pH 7.4), stained with 1% OsO_4 and 1.5% $K_3Fe(CN)_6$, and embedded in an agarose gel for sectioning and dehydration. For MTT assays and confocal microscopy, highly concentrated suspensions of folate-conjugated nanostars (initial O.D. 8, ~4.4 mg/mL) were added to plates containing KB cells to a final concentration of 10 μg/mL, then incubated for 12 h at 37 °C in a 5% CO_2 atmosphere. MTT assays ($N = 20$) were run according to a standardized procedure,[23] using a protective film to prevent evaporation-induced losses in volume and with corrections for nanostar extinctions at the reader wavelength (570 nm). Student *t*-tests were conducted using two-tailed probability values.

Results and Discussion

Magnetically responsive nanostars were prepared by a seeded growth method, starting from core−shell Au@Fe_3O_4 nanoparticles (see Experimental Section). This procedure yielded multiarmed, polycrystalline Au nanostars with 13-nm Fe_3O_4 cores and an average span of 100 nm (Figure 2a,b). Optical extinction spectroscopy of an aqueous dispersion of nanostars produced bimodal resonance bands in the visible and NIR region; the broad linewidths reflect a distribution of resonances due to structural heterogeneity (Figure 2c). Earlier spectroscopic analyses of single nanostars by Hafner and co-workers revealed well-defined NIR resonances with narrow linewidths and polarization-dependent scattering, correlated with the dipolar longitudinal (i.e., radial) plasmon modes of nanostar arms aligned with polarized light.[22] This is in accord with our observations: A statistical analysis of 108 nanostars on a glass substrate indicated that 95% of these produced polarization-sensitive scattering when responding to a rotating magnetic field gradient (Figure S1 and Table S1, Supporting Information).

Gyromagnetic contrast is achieved by synchronizing the magnetic moment with polarized excitation or emission. In this regard, anisotropic nanoparticles such as Au nanostars are excellent candidates, as they have recently been shown to support polarization-dependent scattering at NIR frequencies.[22] By subjecting Au nanostars with magnetic cores to a low-strength, rotating magnetic field gradient, we could generate a periodic scintillation (twinkling) at pulse rates defined by the driving frequency. The dynamic scattering properties of individual nanostars were characterized by darkfield microscopy using a polarized broadband excitation source with a long-pass filter ($\lambda_{ex} > 650$ nm), a modified stirring plate with an adjustable rotor frequency ω (up to 4.8 rps), and a high-speed video camera for real-time analysis (see Experimental Section). Nanostars were adsorbed electrostatically onto coated glass substrates, then imaged under darkfield conditions using an oil-immersion objective while subjected to a rotating magnetic field gradient. The nanostars responded freely to the rotating field gradient to produce a periodic modulation in NIR scattering amplitude (Figure 3a), but were essentially stationary with respect to translation (Movies S1 and S2, Supporting Information). The period of the gyromagnetic response scaled linearly with driving frequency ω, indicating that the magnetic moment of the superparamagnetic Fe_3O_4 core provided sufficient torque ($\boldsymbol{\tau} = \mathbf{m} \times \mu_0\mathbf{H}$, where $\mathbf{m}$ is the magnetic moment at $\mathbf{H}$) to overcome frictional drag.

Fourier transform of the gyromagnetic signals from individual nanostars revealed a signature frequency response at 2ω, corresponding to the rate at which the radial plasmon resonance aligned with the polarization axis (Figure 3b,c). This periodic scattering provides the basis for enhanced optical contrast via frequency-domain imaging: Fourier analysis of the pixelated frames produces a power density map with maximum signal intensity at 2ω, whereas off-resonant frequencies ($\Delta\omega \geq 0.1$ Hz) generate little to no contrast (Figure 3d). Unlike other forms of Fourier-domain imaging which are based on spectroscopic discrimination,[19] the frequency component in gyromagnetic imaging is generated by an external magnetic field gradient and thus orthogonal to the optical input frequency.[15]

While the 2ω signal is characteristic of gyromagnetic imaging, a significant fraction of nanostars also feature the fundamental

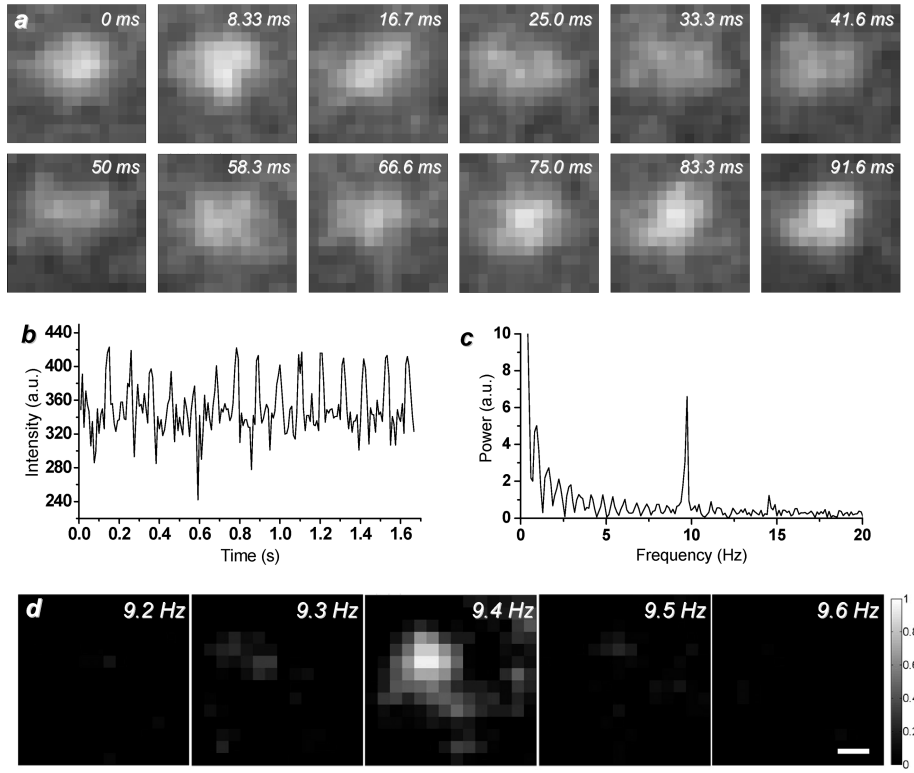

Figure 3. Gyromagnetic imaging of Au nanostars. (a) Series of polarized scattering images of a single nanostar illuminated under darkfield conditions (λ_{ex} > 650 nm) in the presence of a rotating magnetic field gradient (4.7 Hz, B = 80 G); (b) modulation of polarized scattering intensity in real time; (c) power spectrum of rotating nanostar with a characteristic peak at 2ω (9.4 Hz); (d) power density maps (Fourier-domain images) of nanostar in the frequency range of 9.2−9.6 Hz (92 nm/pixel, bar = 200 nm).

mode (ω) or higher-order harmonics (4ω) in their power spectra (Figure S2, Supporting Information). Nanostars with significant ω modulation typically also display the 2ω mode but may exhibit an asymmetric scattering response every 180°, possibly caused by an uneven canting of the rotation axis relative to the image plane. Gyromagnetic signals at higher harmonics are most likely generated by perturbations in angular velocities due to interactions between nanostars and their local environments, such as periodic bumps against nearby objects during gyration.

Gyromagnetic anisotropies are also evident in the dynamic scattering response of "tethered" nanostars that are loosely attached to the polymer-coated substrate, and exhibit a translational orbit in response to the rotating magnetic field gradient (Figure 4). Spatiotemporal mapping of the particles reveals orbital trajectories whose radii vary commensurately with ω, presumably due to the change in centripetal force (Figure 4a and Web-Enhanced Object 1). The elastically tethered nanostars also produce a temporal modulation in scattering that correlates directly with orbital motion, allowing us to further examine the basis for nanostar twinkling. In the case above, the complete spatiotemporal and intensity modulation of the tethered nanostar can be described as a harmonic function $f(x,y,A,t)$ and rendered in 3D as a lissajous, with the upper and lower values of x coinciding with the relative maxima for A (Figure 4b). Fourier analysis of the spatiotemporal domain in one dimension ($f(x,t)$ or $f(y,t)$) produces a major peak corresponding to the driving frequency ω (Figure 4c,d), whereas the time-dependent amplitude function $f(A,t)$ is characterized by a bimodal resonance at ω and 2ω (Figure 4e,f). Fourier-domain mapping of frequency-selective responses reveal two well-resolved signals at ω corresponding to the bimodal scattering maxima in Figure 4b, but a single peak at 2ω (Figure 4g,h). A linescan analysis reveals the latter to be localized in between the ω-mode maxima, indicating that the second-harmonic signal is generated by the spatial overlap of ω-selective peaks with a 180° phase relation (Figure 4i). This confirms that despite their more complex trajectories, the gyromagnetic signals of the tethered nanostars can produce similar frequency-domain images as those which appear to have a constant position.

To evaluate gyromagnetic imaging as a mechanism for enhancing contrast in biological settings, the nanostars were internalized by tumor cells at a low particle density and imaged by polarized darkfield microscopy.[24] Nanostars were introduced to KB cells both in unfunctionalized (CTAB-depleted) form and as folic acid conjugates, the latter typically resulting in higher uptake efficiencies based on receptor-mediated endocytosis.[25] Cells incubated with unfunctionalized nanostars for 12−24 h were examined by TEM, which revealed the nanostars to be compartmentalized as clusters within vacuoles, even at low loading levels (Figure 5).

KB cells with low particle loadings were exposed to a polarized NIR laser beam (λ_{ex} = 780 nm) for selective excitation of the internalized nanostars, whose scattering could be visualized under both conventional (time-domain) and gyromagnetic imaging conditions (Figure 6a−c). Selective Fourier-domain imaging maximizes the peak signal intensity relative to the average time-domain signal, while simultaneously reducing

(24) Au nanostars have recently been used as intracellular imaging probes using cross-polarization microscopy, although with visible rather than NIR wavelengths for excitation. Aaron, J.; de la Rosa, E.; Travis, K.; Harrison, N.; Burt, J.; José-Yacamán, M.; Sokolov, K. *Opt. Express* **2008**, *16*, 2153–67.

(25) Antony, A. C.; Low, P. S. *Adv. Drug Delivery Rev.* **2004**, *56*, 1055–58.

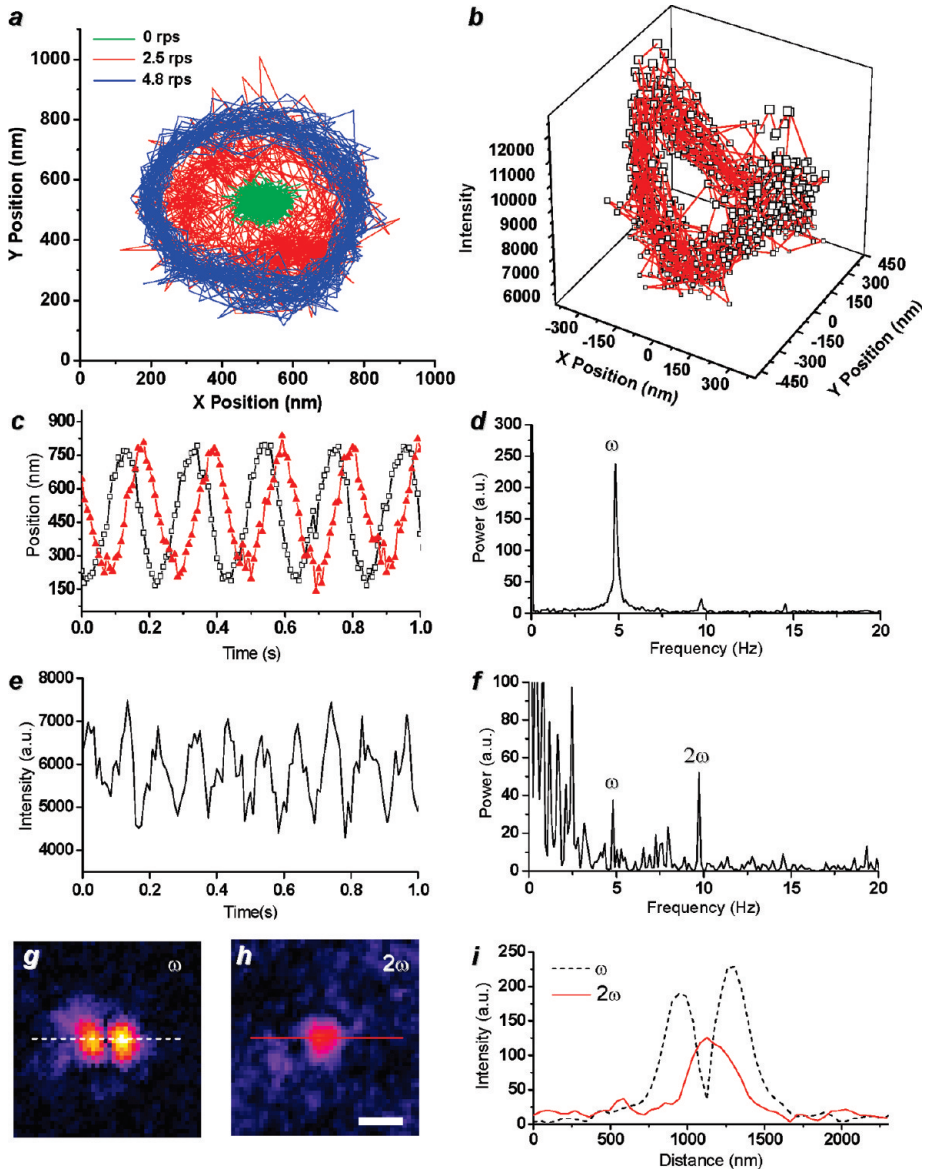

Figure 4. Gyromagnetic scattering from tethered nanostar ($\lambda_{ex} > 650$ nm). (a) Trajectory in the *xy* plane at $\omega = 0$, 2.5, and 4.8 Hz; (b) spatiotemporal distribution of nanostar versus scattering amplitude; (c) nanostar position along *x* (open black squares) or *y* (red triangles) with a rotational orbit of 4.8 rps; (d) Fourier transform of $f(x,t)$; (e) scattering amplitude *A* at 4.8 Hz (acquired over a 4.25 × 4.25 μm^2 region); (f) power spectrum of scattering intensity; (g,h) Fourier-domain images of tethered nanostar at ω and 2ω, respectively (bar = 1 μm); (i) linescans of images g and h.

Ⓦ See Web-Enhanced Object 1 for polarized scattering of tethered nanostar orbiting at 2.5 Hz (0−5 s), 4.8 Hz (6−15 s), and at rest (16−17 s).

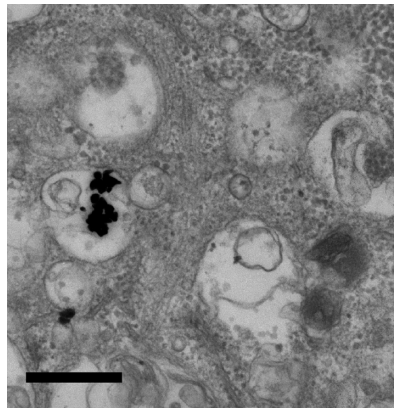

Figure 5. TEM image (Philips CM-100, 80 kV, ×28 500) of unmodified nanostars internalized by KB cell after 24-h incubation (bar = 500 nm).

background noise. Fourier transform of gyromagnetic signals acquired over 800 frames (6.67 s) produced a 2ω-selective image with peak SNR on the order of 2000 (66 dB) and peak signal-to-background ratio (SBR) in excess of 10^4. In comparison, the averaged time-domain image taken from the same data produced peak SNR and SBR values on the order of 110 (41 dB) and 200, respectively. Fourier-domain imaging also provides sharper resolution, and reveals at least two groups of signals within the cluster (Figure 6c,d). These can be attributed to nanostars with independent gyromagnetic activities, as deduced by the phase difference in their frequency-modulated scattering amplitudes (Figure 6e).

Gyromagnetic imaging has the unique advantage of elucidating weak signals embedded within a complex and highly scattering medium. Switching the excitation source from a monochromatic NIR laser diode to a halogen lamp with a long-pass filter ($\lambda > 650$ nm) reduces the signal strength and also

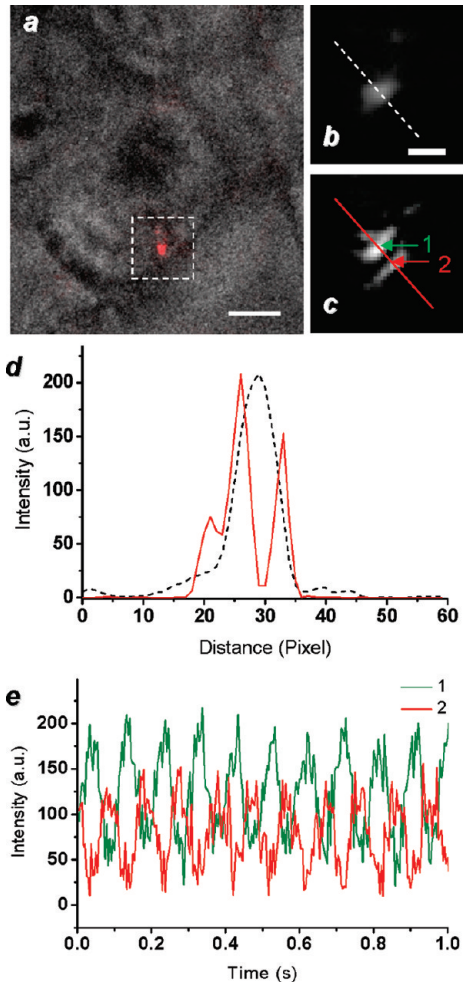

Figure 6. Gyromagnetic detection of Au nanostars in tumor cells, using monochromatic laser excitation (λ_{ex} = 780 nm). (a) Polarized scattering from nanostars (red) in KB cell, imaged in transmission mode (gray, bar = 5 μm); (b) time-averaged image of internalized nanostars, enlarged from inset in (a) (bar = 2 μm); (c) Fourier-domain image (2ω = 9.4 Hz) of internalized nanostars over same area; (d) intensity linescans of time-averaged image (dashed) versus Fourier-domain image (solid red); (e) modulation of polarized scattering intensity in real time from nanostars in neighboring regions within (c), identified as 1 and 2 (green and red arrows, respectively).

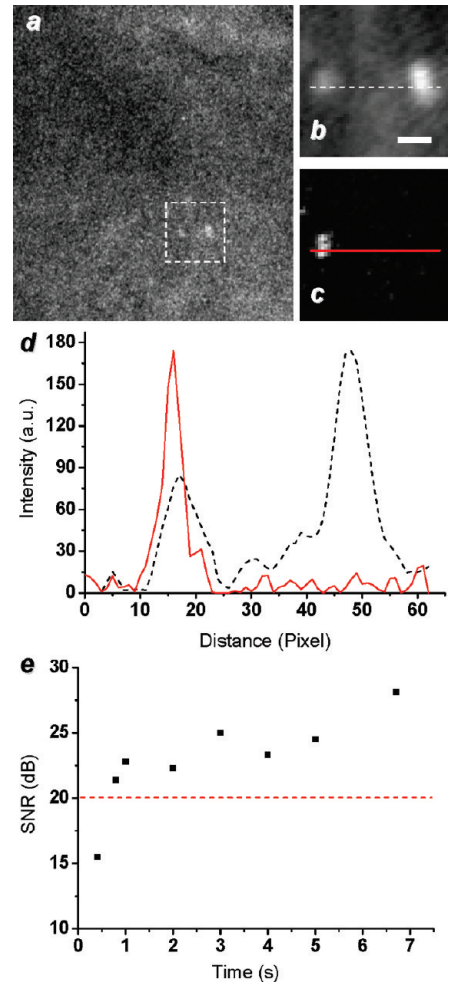

Figure 7. Gyromagnetic detection of Au nanostars in tumor cells, using broadband excitation (λ_{ex} > 650 nm). (a,b) Time-domain scattering images from nanostars in KB cell, with enlarged view of inset (bar = 2 μm); (c) frequency-domain image (2ω = 9.4 Hz) over same area as in (b); (d) intensity linescans from (b) and (c); (e) peak SNR values by Fourier-domain imaging as a function of acquisition time; dashed line represents threshold of acceptable signal quality (20 dB).

produces a substantially noisier background, to the extent that the nanostars can be outshone by other scattering bodies (Figure 7a,b). Despite this, the magnetically responsive nanostars could be unambiguously identified by gyromagnetic signaling. In the example shown (800 frames acquired over 6.67 s, 2ω = 9.4 Hz), Fourier-domain imaging provided a significant increase in peak intensity at the characteristic 2ω response while effectively suppressing signals from invariant or aperiodic scatterers (Figure 7c,d); the gyromagnetic signals had peak SNR and SBR values of 28.1 dB and 36.3, respectively. In comparison, time-averaged signals from the same data set exhibited peak SNR and SBR values of 15.9 dB and 2.0, well below an acceptable level of image quality. We have found gyromagnetic imaging to yield reproducibly detectable signals (SNR > 20 dB, SBR > 12) in just four cycles, enabling nanostars to be clearly resolved in under 1 s (Figure 7e).

It is important to note that the internalized nanostars do not cause any significant loss in cell viability at the concentrations and driving frequencies used in this study, despite their spicular nature. KB cells incubated with folate-conjugated nanostars (10 μg/mL) for 12 h at 37 °C were observed to have accumulated roughly 10^3 nanostars, estimated from two-photon excited luminescence (TPL) signals using multiphoton confocal microscopy (Figure 8a).[4,9,11] Cells with internalized nanostars were exposed to a 80-G magnetic field rotating at 4.7 Hz for 2 h, then incubated for another 24 h prior to a cell proliferation assay based on mitochondrial activity (MTT oxidation). Cells that were loaded with nanostars and subjected to rotating magnetic field gradients were just as viable as those not exposed to magnetic fields (p = 0.999, df = 19, Figure 8c). In fact, the uptake of nanostars correlated with significantly *higher* rates of cell proliferation, relative to that of cell populations without nanostars (p = 0.005, df = 19). Treating fixed KB cells with fluorescent anti-α-tubulin revealed the TPL signals to be closely associated with the microtubule network (Figure 8b), suggesting the possibility that the nanostars may impart some influence on cell growth through cytoskeletal filaments. While further studies are needed to elucidate this stimulatory effect, this study clearly shows that the uptake of gyromagnetically active nanostars does not lead to cell injury, even with exposure to low-frequency magnetic field gradients.

In summary, plasmon-resonant nanostars with superparamagnetic cores can support a dynamic optical imaging

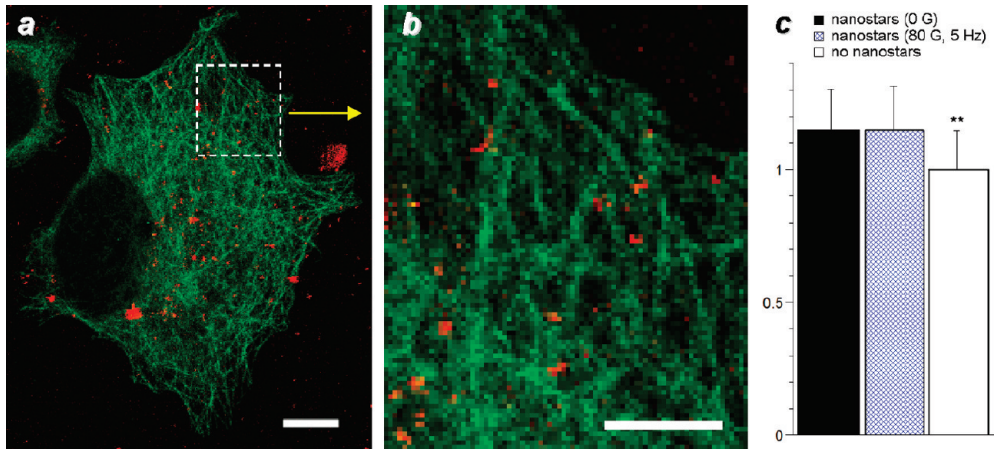

Figure 8. (a,b) Confocal TPL images of internalized nanostars in KB cells (red), in close association with microtubules (green), visualized by immunohistochemical labeling (bar = 2 μm for a, 1 μm for b). (c) Results of MTT assay, indicating that the gyromagnetic activity of internalized nanostars (80 G, ω = 5 Hz) had no significant effect on cell viability, whereas nanostar uptake significantly increased cell proliferation relative to control populations (**, p = 0.005, df = 19).

modality, based on their gyration in response to a rotating magnetic field gradient. Polarized NIR excitation produces a periodic scattering signal with a characteristic 2ω response, which can then be converted into Fourier-domain images with improvements in SNR of up to 25 dB, relative to time-domain images. Further enhancement in image quality is possible through the use of window functions, or simply by increasing the acquisition time. The large enhancements in optical contrast are comparable to that afforded by modalities using multiphoton confocal microscopy, but the gyromagnetic scattering signals are collected using conventional microscope optics. These studies demonstrate that gyromagnetic signaling provides a simple yet practical mechanism for generating optical contrast inside of cells or other complex media, one that is orthogonal and complementary to other methods of signal modulation or noise reduction.

Acknowledgment. The authors gratefully acknowledge the National Institutes of Health for financial support (A.W., EB001777; K.R., GM083296), Dr. Deborah Sherman for TEM sample preparation and analysis, Jenny Sturgis for assistance with confocal fluorescence microscopy, and Prof. Stephen Boppart, Dr. Amy Oldenburg, (University of Illinois), and Prof. Charles Bouman (Purdue University) for helpful discussions. ImageJ software can be obtained free of charge at http://rsb.info.nih.gov/ij.

Supporting Information Available: Schematic of experimental setup, distribution of frequency selections, SNR values in the gyromagnetic responses of nanostars, and movies of nanostars gyrating at 4.8 Hz. This material is available free of charge via the Internet at http://pubs.acs.org.

JA901562J